Indian Journal of Biochemistry & Biophysics
Vol. 61, November 2024, pp. 740-755
DOI: 10.56042/ijbb.v61i11.12051

Molecular docking and dynamics analysis to reveal the therapeutic potential of Dostarlimab against novel immune targets in liver cancer

Swetha Pulakuntla[1], Shri Abhiav Singh[2], Gouthami Kuruvalli[1], Althaf Hussain Shaik[3] & Vaddi Damodara Reddy[1]*

[1]School of Applied Sciences, REVA University, Bangalore-560 064, Karnataka, India

[2]Department of ISRM, Indian Council of Medical Research, NewDelhi-110 029, Delhi, India

[3]Department of Zoology, College of Science, King Saud University, Riyadh-11451, Saudi Arabia

Received 26 June 2024; *revised 22 August 2024*

Computational approaches leveraging large-scale data validation play a pivotal role in advancing immunotherapies. The identification of novel immune targets and the development of potential immune checkpoint inhibitors (ICIs) are crucial for improving cancer treatment outcomes. In this study, we focused on Dostarlimab, a monoclonal antibody targeting the PD-1/PDL1 pathways in cancer, as a potential ICI. The aim of this study was to use bioinformatics analyses to identify immune targets and assess the efficacy of Dostarlimab against these targets. Specifically, we focused on six immune targets: PDL1, AURKA, MELK, NCAPG, PBK, and RACGAP1. Large-scale gene expression studies were performed to identify potential immune targets. The interaction of Dostarlimab with the six chosen targets was assessed through molecular docking. Protein–protein interaction (PPI) simulations were performed using the ClusPro webserver, and molecular dynamics (MD) simulations were conducted using Desmond software. Our results demonstrated that among the selected immune targets, PDL1, a well-known target, exhibited a relatively weak interaction with Dostarlimab. In contrast, the other five targets (AURKA, MELK, NCAPG, PBK, and RACGAP1) showed robust affinity for Dostarlimab based on molecular docking and dynamic simulations. This study suggested that Dostarlimab, an FDA-approved drug and an inhibitor of PD1/PDL1 immunotherapy, has promising potential for use against a panel of immune targets associated with liver cancer. Although PDL1 is a recognized immune target, our findings suggest that the selected novel immune targets may improve therapeutic outcomes. Clinical studies are warranted to validate these findings and establish the reliability of predictive immune targets for the development of effective ICIs for liver cancer patients.

Keywords: Hepatocellular carcinoma, Immune therapy, Immune checkpoint inhibitors, Immune targets, Molecular docking, Molecular simulations

In 1986, the US Food and Drug Administration (FDA) approved the first immunotherapy drug, an antitumor cytokine called interferon-2alpha (IFN-2α), for leukemia treatment[1]. Following studies indicating significant efficacy in the acute stage of leukemia, the FDA granted approval for the use of IFN-2α in the treatment of 3rd-stage melanoma in 1995. Subsequently, in 1998, it was licensed for the treatment of both melanoma and renal cell carcinoma. Interleukin-2 (IL-2), recognized as a T-cell growth factor, exhibits immunological modulation that stimulates T-cell proliferation[2]. Notably, IFN-2α has reached FDA approval as the second most common cytokine-based anticancer drug after IFN-2α[3,4].

The emergence of immune checkpoint inhibitors (ICIs) as pivotal agents in cancer treatment has led to the development of immunotherapies and various formulations for standard cancer therapy[5]. Immune checkpoint inhibitor therapies have focused on tumor cells and can be effectively recognized and knocked down by the immune system. Blocking ICI in human cancer is called immune therapy[6]. The most well-studied ICIs are programmed cell death 1 (PD1), programmed cell death 1 ligand (PDL-1), and cytotoxic T lymphocyte-associated antigen 4 (CTLA4)[7-10]. Another new group, the ICI lymphocyte activation gene 3 (LAG-3) group, was first reported by a French immunologist in 1990. Its transmembrane protein is located in the extracellular and cytoplasmic regions and is closely related to the prognosis of human cancers. Its expression is positively correlated with the development of human tumors, such as lung and hepatocellular carcinoma[11]. However, due to the limitations of treatment and the low response of cancer patients, there is a need to increase the

*Correspondence:
Phone: +91-9502639348 (Mob)
E-mail: reddidamodar@gmail.com

significant discovery of antibody drugs and novel immune targets for specific cancer immunotherapies[12].

On August 7, 2021, the FDA approved Dostarlimab (Jemperll), a monoclonal antibody for advanced deficient mismatch repair (dMMR) endometrial cancer. Dostarlimab works on all types of dMMR and microsatellite instability (MSI) tumors. Abnormal DNA function should be restored to maintain cell health[13]. In 2022, Dostarlimab, a PD-1 inhibitor, was reported to have a long-lasting effect on dMMR in patients with rectal cancer. A clinical trial (NCT04165772) showed promise for determining what drives cancer therapy[14]. Dostarlimab can bind to PD-1 on T cells and block interactions; both ligands are PD-L1 and PDL2, which activate the immune response. This drug functions as a natural antitumor response in cancer treatment; it is given as an intravenous infusion for 30 min every 3 or 6 weeks, depending on the cycle[15].

Based on research reports our interest of the study is Dostarlimab interacting with immune targets, the heavy chain of Dostarlimab is responsible for inhibiting PDL1 binding, while the light chain is likely involved in this blockade[16,17]. Crucial for drug binding, Dostarlimab's high-affinity conformational changes occur in the BC, CD, and FG loops of PD-1, distinguishing its mechanism from that of nivolumab and pembrolizumab[18]. The structural changes are unclear, but known epitopes might show critical efficacy for cancer tumors with different antibodies. However, antibodies that block PD-1 and PDL1 have similar effects[19]. Therefore, the drug Dostarlimab targets and blocks the interaction of PD-1/PDL1 to promote an immune response against cancer cells. Drugs known as immune checkpoint inhibitors could show promising activity in liver cancer[20]. In this research, we performed Dostarlimab molecular docking and simulation interactions against unknown immune targets and compared them with those of the known immune target PDL1[21].

Materials and Methods

Protein data retrieval

The antigen (Ag) targets were selected based on RNA sequence data from our earlier research work, as referenced in Pulakuntla *et al*[22]. The protein sequences of the selected targets, Aurora kinase A (AURKA) (UniProt ID: O14965), Maternal embryonic leucine zipper kinase (MELK) (UniProt ID: Q14680), Condensin complex subunit 3 NCAPG (UniProt ID: Q9BPX3), Lymphokine-activated killer T-cell-originated protein kinase (PBK) (UniProt ID: Q96KB5), and RacGTPase-activating protein 1 (RACGAP1) (UniProt ID: Q9H0H5), were retrieved from the UniProt database in fasta format (https://www.uniprot.org/)[23]. In recently published research, we selected the potential antibody (Ab) Dostarlimab (an immune checkpoint inhibitor)[20].

Functional antigen prediction and antibody modeling

In silico screening of gene targets provides information about most protective antigen identification with vaxiJen 2.0 (http://www.ddg-pharmfac.net/vaxijen/VaxiJen/VaxiJen.html)[24]. It was developed for antigen classification based on the physicochemical properties of the protein sequence. The five protein targets were predicted based on the predefined cutoff rank as protective antigens or nonantigens. The immunogenic receptors PDL1 (PDB ID: 4Z18), AURKA (PDB ID: 2J4Z), MELK (PDB ID: 4IXP), NCAPG (PDB ID: 6IGX), PBK (PDB ID: 5J0A), and RACGAP1 (PDB ID: 2OVJ) were downloaded from the PDB database (https://www.rcsb.org/). The light and heavy chains of the antibody Dostarlimab were downloaded from the PDB database (PDB ID: 7WSL). The target and ligand structures were downloaded and subsequently prepared using Maestro software. The protein structure, which included missing loops, underwent loop modeling using the Swiss Model Server (https://swissmodel.expasy.org)[25]. In the loop modeling process, we employed a user-specific template method, using the same PDB ID as the template for the respective protein. The resulting fully prepared structures were then utilized for further analysis. Dostarlimab high-affinity conformational receptors C and A are heavy and light chains, respectively.

Helper T lymphocyte (HTL) epitope analysis

HLA (human leukocyte antigen) class II epitope analysis was performed using NetMHCIIpan version 4.1 (https://services.healthtech.dtu.dk/services/NetMHCIIpan-4.1/)[26]. The FASTA protein sequence was used as input for the analysis of MHC-II molecules. The prediction was performed based on high binding affinity, and the best epitopes were filtered on the basis of the IC_{50} threshold (500 nM) values, were able to forecast all potential mutant epitopes by strong and weak binding affinity since 9-mer peptides may comprise 90% of neoantigens, we exclusively took them into consideration.

ClusPro Protein–protein docking using antibody mode

We used an antigen and antibody docking protocol with the ClusPro server (http://cluspro.bu.edu/)[27]. Cluspro is one of the best servers in the critical assessment of prediction interaction (CAPRI) for protein docking. Protein-protein docking using ClusPro, particularly in antibody mode, is a robust method for predicting the interaction between antibodies and their target antigens. ClusPro is a powerful docking tool that combines rigid-body docking with a clustering algorithm to predict the most likely protein-protein interactions. In antibody mode, ClusPro specifically optimizes the docking process for the interaction between an antibody and its antigen. This mode takes into account the unique structural features of antibodies, such as their variable regions and antigen-binding sites, to improve the accuracy of the docking predictions. The server has different scoring schemes. In this study, the CluSpro server was accessed in antibody mode, where the antibody structure was designated the receptor and the target protein was designated the ligand. One of the great applications of ClusPro is the prediction of structural oligomeric subunits. Upon submission of the data to the Cluspro server, the docking processes were performed, and the results were retrieved and analyzed based on scoring functions, energy minimization, and other relevant criteria. The top-ranking docking models were visualized using Maestro, providing insights into the predicted protein–protein interactions. The ranking prediction of the generated poses was based on the size of the cluster. The manual predictions have been processed based on stability and optimization analysis and, in some cases, based on biological information. Protein–protein docking is more challenging due to the large complex and finding of unknown binding surfaces.

Molecular dynamic simulations

In this study, we employed molecular dynamics simulations using Desmond software[28] to investigate the dynamic behavior of the complex system Dostarlimab interacting with six immune targets (PDL1, AURKA, MELK, PBK, NCAPG, and RACGAP1).For MD simulations, it is essential to select the most representative docking poses to ensure that the simulation results are meaningful and reflective of the actual biological interaction. In practice, the docking poses generated by ClusPro are analyzed and filtered based on criteria such as the binding energy, interface area, and the quality of the predicted interaction. The top-ranked poses are then chosen for further MD simulations. The simulations were carried out at a physiological temperature of 300 K and pressure of 1.01325 bar within a 10 Å cubic box. The OPLS-2005 force field was applied to accurately represent intermolecular interactions, and TIP3P water molecules were used for solvation. The system underwent initial energy minimization to address steric clashes, followed by a gradual release of constraints for system relaxation. Equilibration stages (NVT and NPT) were performed to adjust the temperature and pressure using thermostats and barostats. Subsequently, production MD simulations were conducted for 100 ns, the energies were recorded at 1.2 ps intervals, and trajectories were saved every 100 ps. In this study, the Noose-Hoover chain thermostat method and the Martyna-Tobias-Klein barostat method with isotropic coupling were employed to control the system's temperature and pressure. The equations of motion were integrated using the leap-frog algorithm with a time step of 2 fs, and the cut-off radius for short-range Coulomb interactions was set to 9.0Å[29]. The simulations, which were independently run six times, aimed to explore the stability and dynamics of the Dostarlimab-immune target interactions. The resulting trajectories were analyzed using Desmond's tools, focusing on parameters such as RMSD and RMSF to provide insights into the system's behavior, thus contributing to a comprehensive understanding of the molecular dynamics of the studied complex. Principal component analysis (PCA) and dynamic cross-correlation matrix (DCCM) analysis were conducted utilizing the 'Bio3D' package within the R environment[30].

Results

VAXIJEN antigenic prediction

The selected proteins from early research work on Microarry GEO datasets (AURKA, MELK, NCAPG, PBK and RACGAP1), were retrieved from the UniProt database; these proteins are selected based on primarily involved directly or indirectly in multiple cancer signaling pathways, such as the P53 pathway, Hippo pathway, PI3k-Akt pathway, FOXO pathway, and PI3k-mTOR signaling pathway[31]. Gene selection was based on physicochemical properties, and in the immunogenicity analysis performed by VAXIJEN 2.0, the threshold cutoff value was 0.4 for the 5 immune targets. The predicted strong antigens

identified in (Table 1) were AURKA (0.4829), MELK (0.5048), NCAPG (0.4755), PBK (0.4611), and RACGAP1 (0.6213). Further antigen and antibody structural data files were retrieved from the PDB database.

Helper T lymphocyte (HTL) epitope analysis

In this study, a comprehensive analysis of helper T lymphocyte (HTL) epitopes was conducted, focusing on 15-mer peptides binding to classII MHC molecules. The prediction was performed for nine superfamily alleles: DRB1_0101, DRB1_0301, DRB1_0401, DRB1_0701, DRB1_0801, DRB1_0901, DRB1_1101, and DRB1_150[32]. This analysis aimed to identify potential epitopes within the target proteins. The assessment was based on IC_{50} values, a measure of peptide-MHC binding affinity. The analysis yielded epitope predictions for each target protein, with 79 epitopes for AURKA, 164 epitopes for MELK, 89 epitopes for NCAPG, 79 epitopes for PBK and 181 epitopes for RACGAP1. NetMHCPan 4.0 epitope analysis.

Docking analysis

Docking of the antibody (Dostarlimab PDB ID: 7WSL) against known PDL1 (PDB ID: 4Z18) and 5 other antigens (AURKA (PDB ID: 2J4Z), MELK (PDB ID: 4IXP), NCAPG (PDB ID: 6IGX), PBK (PDB ID: 5J0A), and RACGAP1 (PDB ID: 2OVJ)) was performed with the ClusPro server. The weighted scores of the energy outputs of the clusters are given in (Table 2). Cluster 0 of the PDL and Dostarlimab complex had the lowest energy (-433.9 kcal/mol), Cluster 7 of the AURKA and Dostarlimab complex had the lowest energy (-466.9 kcal/mol), Cluster 16 of the MELK complex had the lowest energy (-466.5 kcal/mol), Cluster 0 of the NCAPG and Dostarlimab complex had the lowest energy (460.2 kcal/mol), Cluster 9 of the PBK and Dostarlimab complex had the lowest energy (-435.1 kcal/mol), and Cluster 1 of the RACGAP1 and Dostarlimab complex had the lowest energy (-460.2 kcal/mol).

The intermolecular interactions observed between the antibody (PDB: 7WSL) and the antigen (PDB ID: 4Z18) in a protein–protein docking study are provided in (Table 3). One notable interaction involves Tyr 100 on the heavy chain, which forms one hydrogen bond with Lys 185 on the antigen. Another interaction Tyr 100 on the heavy chain engages in one hydrogen bond with Asp 138 on the antigen. The tyrosine at position 59 on the heavy chain establishes a hydrogen bond with Glu188 on the antigen. Another tyrosine at position 57 on the heavy chain establishes a hydrogen bond with Gln 107 on the antigen. Ser 56 on the heavy chain establishes a hydrogen bond with Asp 103. Another Ser 52 on the heavy chain establishes a hydrogen bond with Glu 187. Furthermore, Asp 33 on the heavy chain is involved in two hydrogen bonds and two salt bridges with Arg186 and Lys185 on the antigen. The tyrosine at position 32 on the heavy chain forms a hydrogen bond with Asn138 on the antigen. Moving to the light chain (A), Thr94 participates in a hydrogen bond with Lys185 on the antigen. The Ser92 light chain establishes hydrogen bonds with Asn183 on the antigen. Another interaction, Thr53 on the light chain, engages in one hydrogen bond with Lys178 on the antigen. Finally, Trp 50 on the light chain interacts with Lys 178 on the antigen through one hydrogen bond (Fig. 1A).

Table 1 — VAXIJEN antigenic prediction

Protein	Threshold	Protective antigen score	Antigen prediction
AURKA	0.4	0.4829	Probable antigen
MELK	0.4	0.5048	Probable antigen
NCAPG	0.4	0.4755	Probable antigen
PBK	0.4	0.4611	Probable antigen
RCGAP1	0.4	0.6213	Probable antigen

Table 2 — Docking analysis of antigens and antibodies

Antibody	Antigen	Model No.	Docking Score (kcal/mol)
7WSL (Dostarlimab)	4Z18 (PDL1)	0	-433.9
	2J4Z (AURKA)	7	-466.9
	4IXP (MELK)	16	-466.5
	6IGX (NCAPG)	0	-460.2
	5J0A (PBK)	9	-435.1
	2OVJ (RACGAP1)	1	-435.1

Table 3 — Intermolecular interactions between 7WSL and 4Z18

Antibody (PDB: 7WSL)	Antigen (PDB ID: 4Z18)	Specific Interactions
C:Tyr 100	Lys 185	1x hb
C:Tyr 100	Asn 138	1x hb
C:Tyr 59	Glu 188	1x hb,
C:Tyr 57	Gln 107	1x hb
C:Ser 56	Asp 103	1x hb
C:Ser 52	Glu 187	1x hb
C:Asp 33	Arg 186	1x hb, 1x salt bridge
C:Asp 33	Lys 185	1x hb, 1x salt bridge
C:Tyr 32	Asn 138	1x hb
A:Tyr 94	Lys 185	1x hb
A:Ser 92	Asn 183	1x hb
A:Thr 53	Lys 178	1x hb
A:Trp 50	Lys 178	1x hb

*A=Light chain; C=heavy chain; hb=hydrogen bond

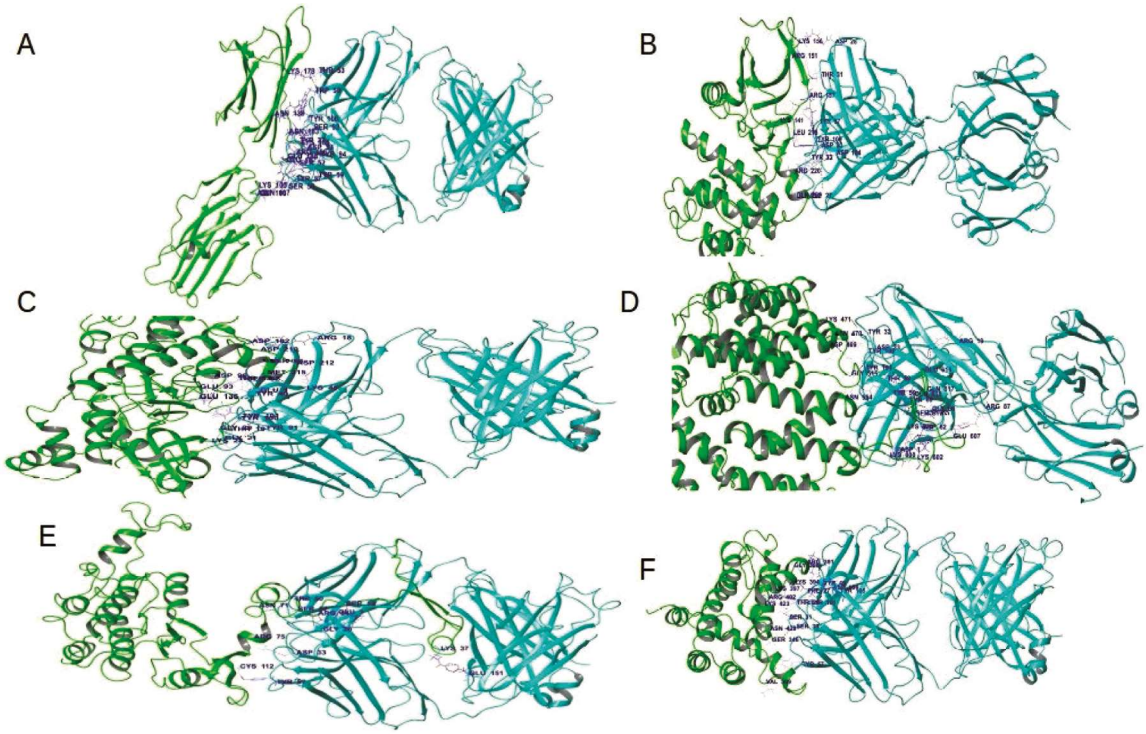

Fig. 1 — Intermolecular interactions between (A) 7WSL and 4Z18, (B) 7WSL and 2J4Z, (C) 7WSL and 4IXP, (D) 7WSL and 6IGX, (E) 7WSL and 5J0A, and (F) 7WSL and 2OVJ, where green indicates 6 immune targets, 4Z18, 2J4Z, 4IXP, 6IGX, 5J0A and 20VJ (Ag), and blue indicates 7WSL (Ab)

The intermolecular interactions observed between the antibody (PDB: 7WSL) and the antigen (PDB ID: 2J4Z) in a protein–protein docking study are provided in (Table 4). One notable interaction involves Asp 104 on the heavy chain, forming one hydrogen bond and one salt bridge with Arg 220 on the antigen. Additionally, Tyr 100 on the heavy chain engages in two hydrogen bonds with Arg137 on the antigen. Another interaction between Tyr 100 and Leu 215 is characterized by a single hydrogen bond. The tyrosine at position 57 on the heavy chain establishes a hydrogen bond with Lys 141 on the antigen. Furthermore, Asp 33 on the heavy chain is involved in two hydrogen bonds and one salt bridge with Arg 137 on the antigen. The tyrosine at position 32 on the heavy chain forms a hydrogen bond with Gln 223 on the antigen. Moving to the light chain (A), Thr 31 participates in a hydrogen bond with Arg 151 on the antigen. Finally, Asp28 on the light chain interacts with Lys156 on the antigen through one hydrogen bond and one salt bridge (Fig. 1B).

Table 4 — Intermolecular interactions between 7WSL and 2J4Z

Antibody (PDB: 7WSL)	Antigen (PDB ID: 2J4Z)	Specific Interactions
C:Asp 104	Arg 220	1x hb, 1x salt bridge
C:Tyr 100	Arg 137	2x hb
C:Tyr 100	Leu 215	1x hb
C:Tyr 57	Lys 141	1x hb
C:Asp 33	Arg 137	2x hb, 1x salt bridge
C:Tyr 32	Gln 223	1x hb
A:Thr 31	Arg 151	1x hb
A:Asp 28	Lys 156	1x hb, 1x salt bridge

*A=Light chain; C=heavy chain; hb=hydrogen bond

The intermolecular interactions observed between the antibody (PDB: 7WSL) and the antigen (PDB ID: 4IXP) in a protein–protein docking study are provided in (Table 5). One notable interaction involves Tyr 101 on the heavy chain, which forms one hydrogen bond with Thr 19 on the antigen. Another interaction Tyr 100 on the heavy chain engages in two hydrogen bonds with Glu 136 and Gly 20 on the antigen. Glu1 on the heavy chain forms one hydrogen bond with Met215 on the antigen. Moving to the light chain, Try 91 participates in a hydrogen bond with Lys 24 on the antigen. The Ser63 light chain establishes hydrogen bonds with Asp102 on the antigen. The Thr 53 light chain establishes hydrogen bonds with GLU 93 on the antigen. Another interaction occurs between Ser 52 and Asp 96 *via* a hydrogen bond. The tyrosine at position 49 on the light chain establishes a hydrogen

bond with Glu 136 on the antigen. Furthermore, Lys 45 on the light chain forms a salt bridge with Asp 212 on the antigen. Finally, Arg 18 on the light chain interacts with Asp 102 on the antigen through two hydrogen bonds and one salt bridge (Fig. 1C).

The intermolecular interactions observed between the antibody (PDB: 7WSL) and the antigen (PDB ID: 6IGX) in a protein–protein docking study are provided in (Table 6). One notable interaction involves Tyr 101 on the heavy chain, which forms one hydrogen bond with Asp 469 on the antigen. Another interaction Tyr 100 on the heavy chain engages through hydrogen bonding with Asn 470 on the antigen. The Arg heavy chain interacts with the Glu 607 antigen *via* one hydrogen bond. Furthermore, Gly66 on the heavy chain forms two hydrogen bonds with Glu618 and Gln617 on the antigen. Another Lys 65 on the heavy chain also forms two hydrogen bonds, and one clashes with Ser 619 and Glu 618 on the antigen. Additionally, Asp 62 on the heavy chain forms three hydrogen bonds, two salt bridges and one clash with Lys 602 and Lys 620 on the antigen. The tyrosine at position 60 on the heavy chain established one hydrogen bond with Glu618 on the antigen. Again, tyrosine at position 59 on the heavy chain forms one hydrogen bond with Asn 554 on the antigen. Thr 58 on the heavy chain forms one hydrogen with Glu618 on the antigen. Asp 33 on the heavy chain established a hydrogen bond with Gly 515 on the antigen. Furthermore, Arg 19 formed one hydrogen bond and one salt bridge with Glu616 on the antigen. Finally, the light chain Asp 1 interacts with Lys 600 on the antigen through one hydrogen bond and one salt bridge (Fig. 1D).

The intermolecular interactions observed between the antibody (PDB: 7WSL) and the antigen (PDB ID: 5J0A) in a protein–protein docking study are provided in (Table 7). One notable interaction involves Glu 151 on the heavy chain, which forms two hydrogen bonds and one salt bridge with Lys 37 on the antigen. Another interaction, Tyr 57 on the heavy chain, engages through hydrogen bonding with Cys 112 on the antigen. The Asp 33 heavy chain interacts through a salt bridge with Arg 75 on the antigen. Furthermore, Gly 26 on the heavy chain forms one hydrogen bond with Ser 57 on the antigen. Another interaction, Glu 1 on the heavy chain, formed three hydrogen bonds, and one clashed with Arg 54 and Ser 54 on the antigen. Finally, only one interaction on the light chain, Trp 50, with Asn 71 on the antigen occurred through one hydrogen bond (Fig. 1E).

Table 5 — Intermolecular interactions between 7WSL and 4IXP

Antibody (PDB: 7WSL)	Antigen (PDB ID: 4IXP)	Specific Interactions
C:Tyr 101	Thr 19	1x hb
C:Tyr 100	Glu 136	1x hb
C:Tyr 100	Gly 20	1x hb
C:Glu 1	Met 215	1x hb
A:Tyr 91	Lys 24	1x hb
A:Ser 63	Asp 102	1x hb
A:Thr 53	Glu 93	1x hb
A:Ser 52	Asp 96	1x hb
A:Tyr 49	Glu 136	1x hb
A:Lys 45	Asp 212	1x salt bridge
A:Arg 18	Asp 102	2x hb, 1x salt bridge

*A=Light chain; C=heavy chain; hb=hydrogen bond

Table 6 — Intermolecular interactions between 7WSL and 6IGX

Antibody (PDB: 7WSL)	Antigen (PDB ID: 6IGX)	Specific Interactions
C:Tyr 101	Asp 469	1x hb
C:Tyr 100	Asn 470	1x hb
C:Arg 87	Glu 607	1x hb, 1x salt bridge
C:Gly 66	Glu 618	1x hb
C:Gly 66	Gln 617	1x hb
C:Lys 65	Ser 619	1x hb
C:Lys 65	Glu 618	1x hb, 1x clash
C:Asp 62	Lys 602	2x hb, 1x salt bridge, 1x clash
C:Asp 62	Lys 620	1x hb, 1x salt bridge
C:Tyr 60	Glu 618	1x hb
C:Tyr 59	Asn 554	1x hb
C:Thr 58	Glu 618	1x hb
C:Asp 33	Gly 515	1x hb
C:Arg 19	Glu 616	1x hb, 1x salt bridge
A:Asp 1	Lys 600	2x hb, 1x salt bridge

*A=Light chain; C=heavy chain; hb=hydrogen bond

Table 7 — Intermolecular interactions between 7WSL and 5J0A

Antibody (PDB: 7WSL)	Antigen (PDB ID: 5J0A)	Specific Interactions
C:Glu 151	Lys 37	2x hb, 1x salt bridge
C:Tyr 57	Cys 112	1x hb
C:Asp 33	Arg 75	1x salt bridge
C:Gly 26	Ser 57	1x hb
C:Glu 1	Arg 54	2x hb
C:Glu 1	Ser 52	1x hb, 1x clash
A:Trp 50	Asn 71	1x hb

*A=Light chain; C=heavy chain; hb=hydrogen bond

The intermolecular interactions observed between the antibody (PDB: 7WSL) and the antigen (PDB ID: 2OVJ) in a protein–protein docking study are provided in (Table 8). One notable interaction involves Try 105 on the heavy chain, forming one hydrogen bond, and two clashes with Arg 391 on the

Table 8 — Intermolecular interactions between 7WSL and 2OVJ

Antibody (PDB: 7WSL)	Antigen (PDB ID: 5J0A)	Specific Interactions
C:Tyr 105	Arg 391	1x hb, 2x clash
C:Asp 104	Lys 394	1x salt bridge
C:Tyr 101	Lys 423	1x hb
C:Tyr 57	Val 509	1x hb
C:Ser 31	Lys 397	1x hb
C:Ser 30	Ser 346	1x hb
C:Thr 28	Arg 402	1x hb
C:Phe 27	Arg 402	1x hb
A:Tyr 49	Gly 388	1x hb

*A=Light chain; C=heavy chain; hb=hydrogen bond

antigen. Another interaction, Asp 104 on the heavy chain, engages through a salt bridge with Lys 394 on the antigen. The Tyr 101 heavy chain interacts through one hydrogen bond with Lys 423 on the antigen. Another Tyr 57 on the heavy chain forms one hydrogen bond with Val 509 on the antigen. Furthermore, the interaction of Ser31 on the heavy chain results in the formation of one hydrogen bond with Lys397 on the antigen. Another Ser30 residue on the heavy chain interacts with Ser346 on the antigen through one hydrogen bond. Thr 28 on the heavy chain forms a hydrogen bond with Arg 402 on the antigen. Furthermore, Phe 27 on the heavy chain established one hydrogen bond with Arg 402 on the antigen. Finally, only one interaction on the light chain, Tyr 49, with Gly 388 on the antigen occurred through one hydrogen bond (Fig. 1F).

All docking complex interactions, distances (Å), and surface complementary data in the 3D structure of the docked antigen, and the antibody binding complex was visualized by Schrodinger's Mastro tool. Dostarlimab and the known immune target PDL1 (4Z18) have a lower binding affinity than other immune targets. The results for all antigen and antibody complexes showed different docking scores, indicating that the docked complexes were strong and stable for immunological responses. Immune targets have good binding affinity for Dostarlimab, so we could consider Dostarlimab a good immune checkpoint inhibitor for the activation of T cells to kill cancer cells, and this antibody inhibitor could act as an immunotherapy in liver cancer patients.

Molecular dynamics and simulation

RMSD

The RMSD values obtained from 100 ns MD simulations provide a dynamic perspective on the stability of the antibody (PDB ID: 7WSL) when bound to different antigens (Fig. 2). This plot indicates the deviation of the atomic positions from the starting structure over the simulation period.

The complex with the antigen 7WSL-2OVJ had the lowest average RMSD of 3.942 Å, suggesting that the antibody maintained a relatively stable conformation throughout the simulation when bound to this particular antigen. The small standard deviation of 0.697 Å implies a consistent and well-defined binding interface, indicating a robust and enduring interaction between the antibody and 7WSL-2OVJ.

Conversely, the complex with the antigen 7WSL-4Z18 exhibited the highest average RMSD of 5.064 Å, indicating a greater degree of structural fluctuation during the MD simulation. This could imply a more dynamic binding interaction, where the antibody experiences significant conformational changes or fluctuations in its interaction with 7WSL-4Z18. The higher standard deviation of 0.884 Å further supports the notion of a less stable binding interface, suggesting greater flexibility or variability in the antibody-antigen interaction.

The intermediate RMSD values observed for the complexes with the antigens 7WSL-2J4Z, 7WSL-4IXP, 7WSL-6IGX, and 7WSL-5J0A indicate varying degrees of binding stability. These complexes exhibit average RMSD values ranging from 4.463 Å to 4.972 Å, reflecting moderate levels of structural fluctuations during the 100 ns MD simulations. The corresponding standard deviations, ranging from 0.657 Å to 1.001 Å, provide insights into the extent of variability in the binding interactions within these complexes.

The RMSD values obtained from 100 ns MD simulations for different antigens binding to the antibody (PDB ID: 7WSL) provide valuable insights into the stability and dynamic behavior of these complexes (Fig. 2). A comparison of the results revealed that each antigen-antibody interaction exhibited unique characteristics during the simulation.

The complex with the antigen 7WSL-2J4Z had the lowest average RMSD of 2.606 Å, indicating a remarkably stable binding interaction. The small standard deviation of 0.189 Å further suggested that the antibody maintained a consistent and well-defined conformation when bound to 7WSL-2J4Z throughout the simulation. Similarly, the complex with the antigen 7WSL-2OVJ demonstrated a low average RMSD (2.873 Å) and a small standard deviation (0.194 Å), indicating stable and uniform binding dynamics.

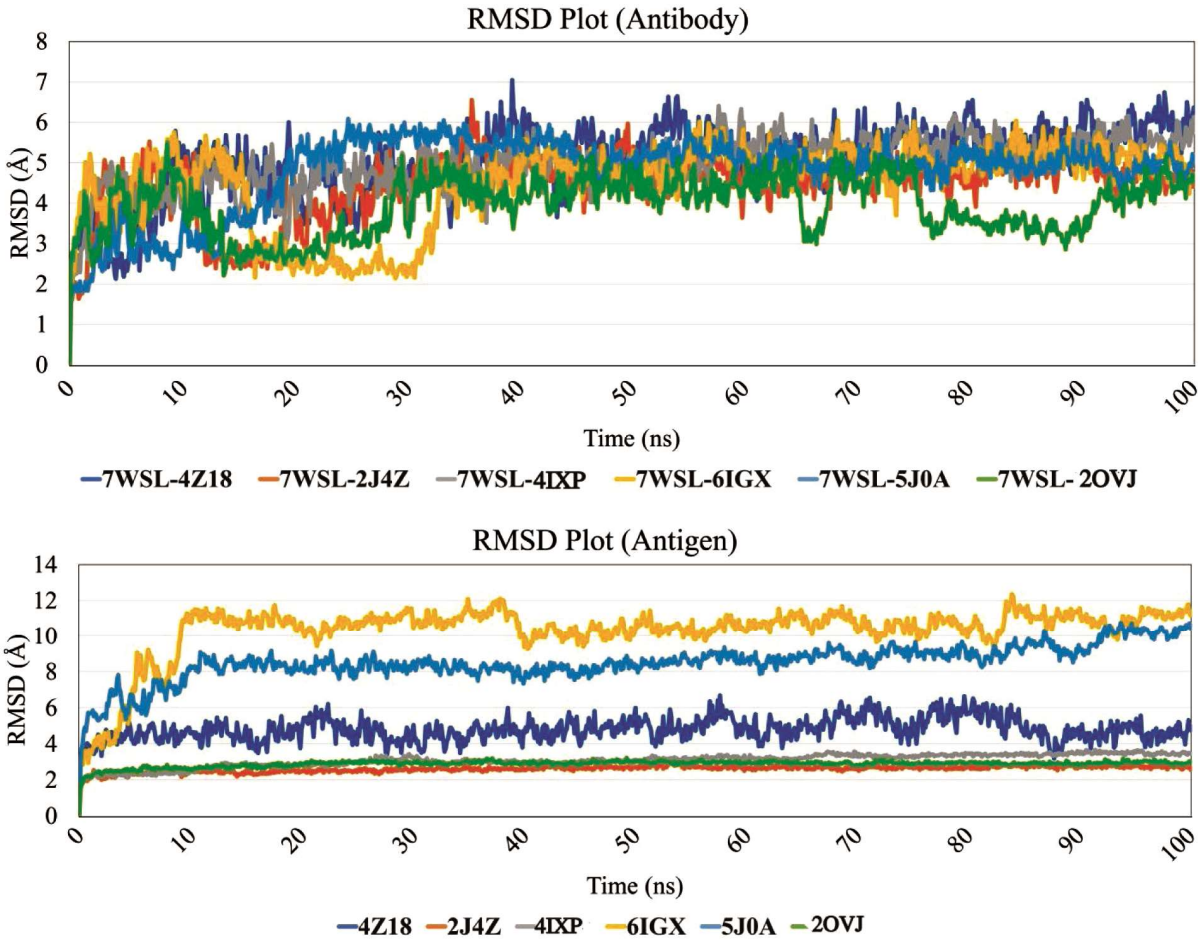

Fig. 2 — The RMSD values obtained from 100 ns MD simulations provide a dynamic perspective on the stability of the antibody (PDB ID: 7WSL) when bound to different antigens (PDB IDs: 4Z18, 2J4Z, 4IXP, 6IGX, 5J0A and 20VJ)

In contrast, the complexes with the antigens 7WSL-6IGX and 7WSL-5J0A showed significantly greater average RMSD values (10.317 Å and 8.512 Å, respectively). The larger standard deviations (1.566 Å and 1.036 Å) associated with these complexes suggest more dynamic and variable binding interactions. These findings imply that the antibody undergoes substantial structural fluctuations when bound to these antigens during the simulated time frame.

Considering both the average RMSD and standard deviation values, it can be concluded that the complexes with the antigens 7WSL-2J4Z, 7WSL-2OVJ and 7WSL-4IXP exhibit greater stability during the 100 ns MD simulation. These complexes maintain lower standard deviations and demonstrate less variability in the binding interface, suggesting a robust and consistent interaction between the antibody and these specific antigens. Conversely, the complexes with the antigens 7WSL-6IGX and 7WSL-5J0A appear to have less stable binding interactions, as reflected by higher average RMSD values and larger standard deviations.

RMSF

Th1e root mean square fluctuation (RMSF) values provide a detailed perspective on the local structural dynamics of the antibody (PDB ID: 7WSL) when interacting with different antigens during a 100 ns MD simulation. Analyzing the RMSF data for each complex revealed distinct pattern of flexibility and fluctuations within the antibody-antigen interfaces (Fig. 3).

The complexes formed with the antigens 7WSL-4Z18 and 7WSL-2J4Z exhibited similar average RMSF values of 2.651 Å and 2.645 Å, respectively. These values suggest moderate local structural fluctuations in the binding interfaces, indicating a balanced degree of flexibility in the antibody-antigen interactions. The corresponding standard deviations of 0.701 Å and 0.709 Å further support the notion of

consistent and comparable local dynamics in these complexes.

In contrast, the complex with the antigen 7WSL-4IXP had a slightly lower average RMSF of 1.840 Å, suggesting reduced local structural fluctuations at the antibody-antigen interface. The smaller standard deviation of 0.538 Å emphasizes the uniformity and stability of the local dynamics in this particular complex. On the other end of the spectrum, the complex with the antigen 7WSL-6IGX displays a higher average RMSF of 2.857 Å, indicating more pronounced local structural fluctuations during the MD simulation. The larger standard deviation of 1.159 Å further highlights the increased variability and heterogeneity in the local dynamics of the antibody when bound to 7WSL-6IGX.

The complex with the antigen 7WSL-4IXP, with the smallest standard deviation of 0.538 Å, showed a more consistent and less variable pattern of local structural fluctuations. In contrast, the complex with the antigen 7WSL-6IGX, characterized by the largest standard deviation of 1.159 Å, exhibited more diverse and variable local structural dynamics. The RMSF analysis underscores the varying degrees of flexibility within the antibody-antigen complexes. While the complexes with the antigens 7WSL-4Z18 and 7WSL-2J4Z demonstrated moderate and comparable local fluctuations, the complex with the antigen 7WSL-4IXP exhibited reduced variability, and the complex with the antigen 7WSL-6IGX displayed greater local dynamics.

The RMSF values, representing the local structuraldynamics of the antibody (PDB ID: 7WSL) when bound to different antigens during a 100 MD simulation (Fig. 4), provide nuanced insights into the flexibility and stability of the antibody–antigen complexes. The complex with antigen 7WSL-4Z18 exhibits an average RMSF of 3.169 Å, accompanied by a standard deviation of 1.010 Å. In comparison, the complex with antigen 7WSL-2J4Z displays a slightly lower average RMSF of 2.260 Å with a standard deviation of 0.641 Å. Despite the similar average RMSF values, 7WSL-4Z18 shows a higher standard deviation, implying more variability in local fluctuations. This suggests that while both complexes experience moderate local structural dynamics, 7WSL-2J4Z displays a more consistent pattern of fluctuations.

In the case of the complex with the antigen 7WSL-4IXP, a notably lower average RMSF of 1.901 Å and a small standard deviation of 0.850 Å are observed. These values indicate that this complex has a relatively stabilized antibody-antigen interface, with reduced local fluctuations and a consistent pattern of structural dynamics. The complexes with the antigens 7WSL-6IGX and 7WSL-5J0A exhibited higher average RMSF values of 3.629 Å and 2.957 Å, respectively. The standard deviation for 7WSL-6IGX is 1.280 Å, indicating relatively variable local structural dynamics, while 7WSL-5J0A displays a larger standard deviation of 2.137 Å, suggesting increased variability and flexibility in the antibody-antigen interface. The complex with the antigen 7WSL-2OVJ demonstrates an intermediate average RMSF of 2.040 Å with a relatively low standard

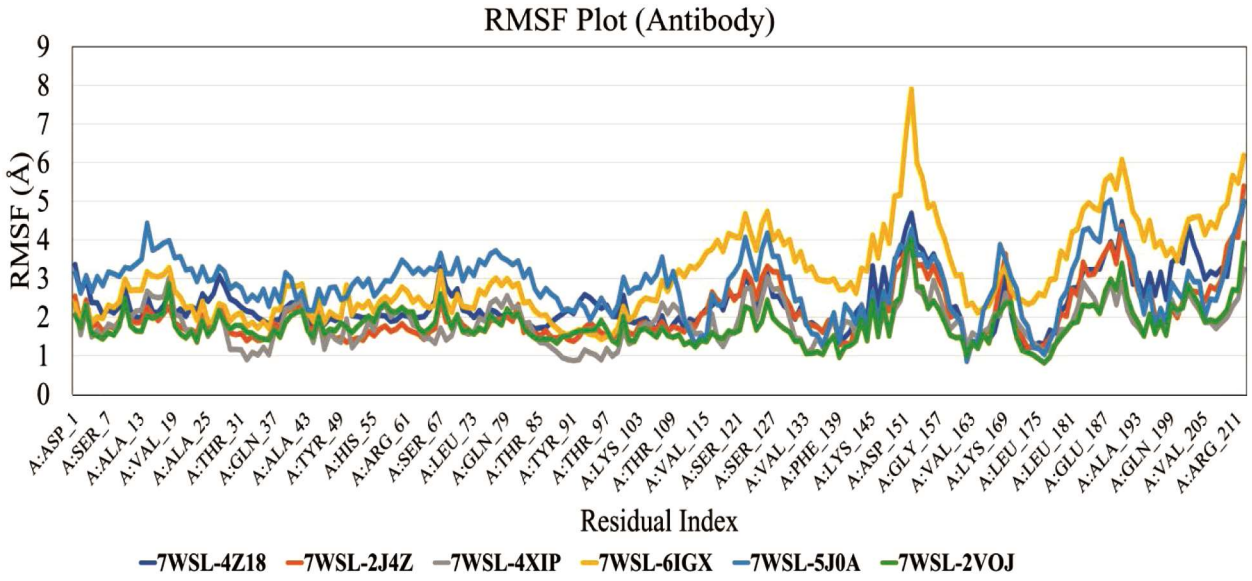

Fig. 3 — The RMSF data of each complex reveal distinct patterns of flexibility and fluctuations within the antibody–antigen interfaces

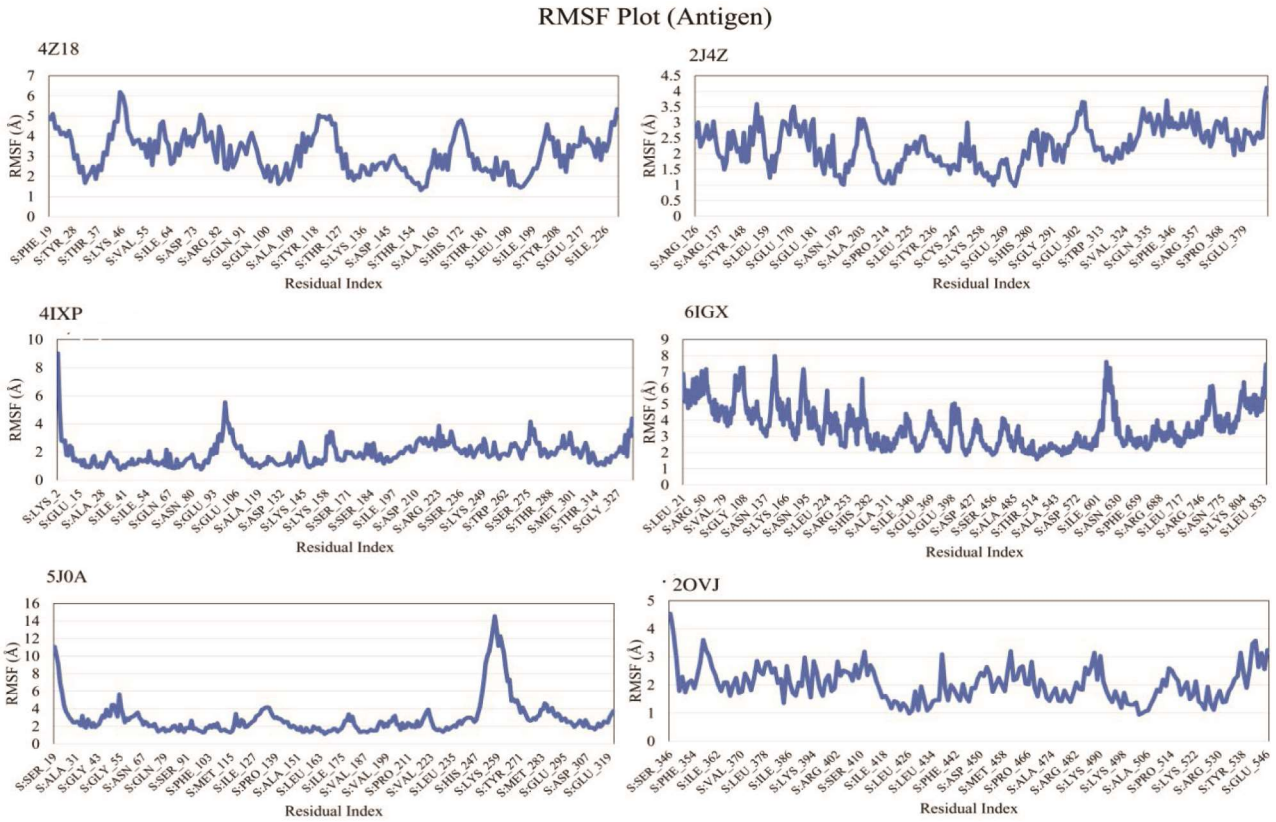

Fig. 4 — The RMSF values, representing the local structural dynamics of the antibody (PDB ID: 7WSL) when bound to different antigens (PDB IDs: 4Z18, 2J4Z, 4IXP, 6IGX, 5J0A and 20VJ), were obtained during 100 MD simulations

deviation of 0.610 Å. This implies a moderate level of local fluctuations, and the small standard deviation suggests a more consistent pattern of dynamics in this complex.

Comparing these antigen-antibody complexes with the RMSF values of the antibody alone revealed that the presence of antigens influences the local dynamics of the antibody. The antigens 7WSL-4IXP and 7WSL-2OVJ appeared to stabilize the antibody, while the antigens 7WSL-6IGX and 7WSL-5J0A induced greater flexibility. These findings contribute to a comprehensive understanding of how different antigens impact the dynamic behavior of antibody-antigen interactions during MD simulations, shedding light on the complex and dynamic nature of immune responses.

Dynamic analysis with PCA and the DCCM

In this study, essential dynamics analysis was conducted on each trajectory acquired from protein–protein complexes using Schrödinger's script, generating principal components (PCs) from each MD simulation trajectory. The distribution of PCs upon Dostarlimab binding was displayed using the top two PCs (PC1 and PC2) in comparison to the immune target protein structures 7WSL-4Z18, 7WSL-2J4Z, 7WSL-4IXP, 7WSL-6IGX, 7WSL-5J0A, and 7WSL-2OVJ (Fig. 5A-F). According to these results, PCs with distributions exhibit considerable changes in protein structure upon Dostarlimab binding, signifying dynamics in the immune targets and Dostarlimab complex, which could lead to immune activity involving T cells in the immune system. This finding illustrates how the association between immune targets and Dostarlimab residues supports the PC results. Porcupine plots were constructed from PC1 and PC2 data, and overlay plots of all six systems (7WSL-4Z18, 7WSL-2J4Z, 7WSL-4IXP, 7WSL-6IGX, 7WSL-5J0A, and 7WSL-2OVJ) for each antigen dataset were constructed to further illustrate the directionality of motion and changes upon antibody binding. This research revealed significant differences in the dynamics of protein–protein complexes. Changes in the position, number, and magnitude of immune targets arising from each atom can be analyzed. When Dostarlimab binds to each immune target, it can activate T cells in the immune system, potentially aiding in killing

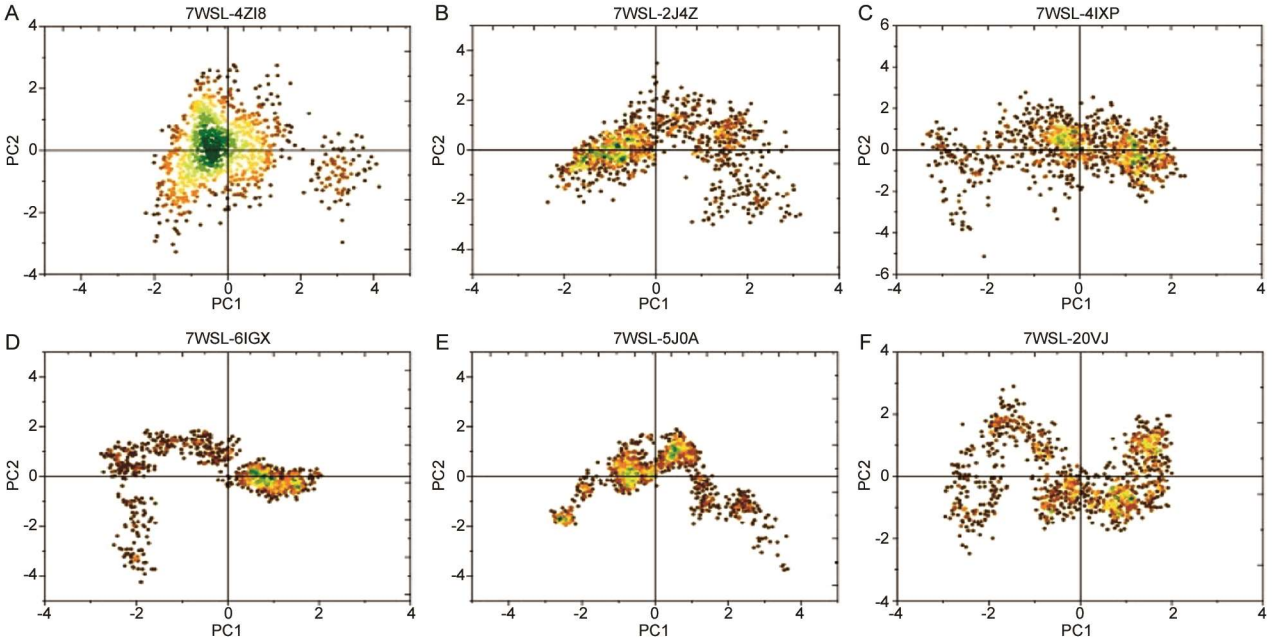

Fig. 5 — Projection of C alpha atoms in the essential subspace along with principal components (PC1, PC2) obtained from the MD trajectories of six immune targets and Dostrolib complexes (A) 7WSL-4Z18, (B) 7WSL-2J4Z, (C) 7WSL-4IXP, (D) 7WSL-6IGX, (E) 7WSL-5J0A and (F) 7WSL-2OVJ

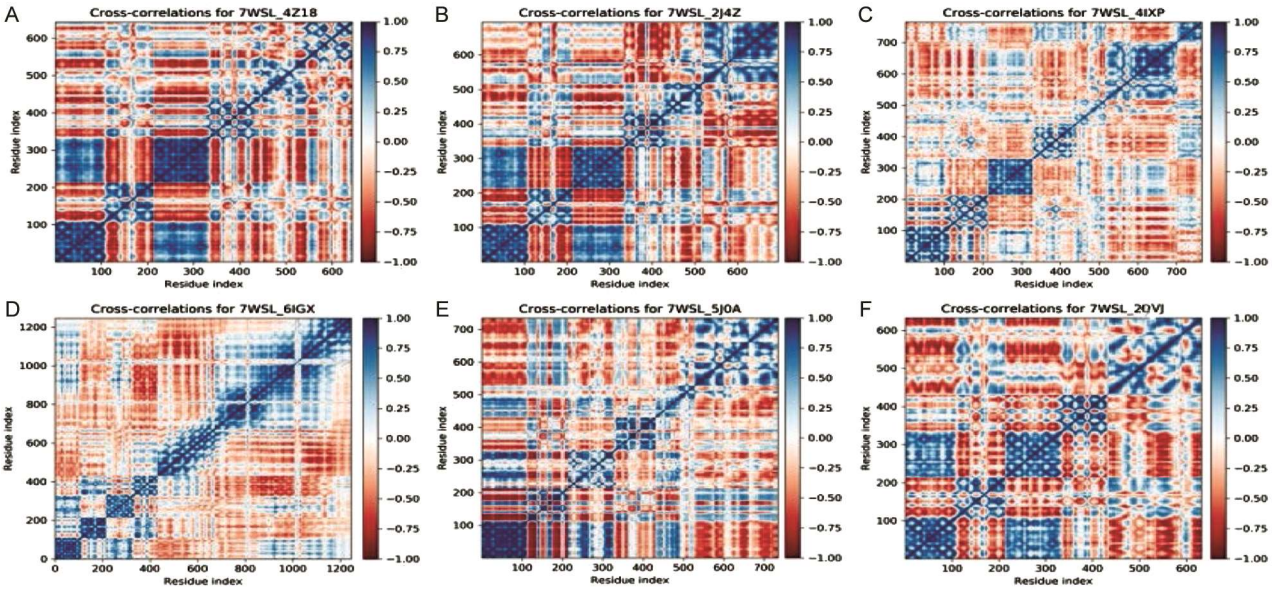

Fig. 6 — DCCM analysis for the six systems.(A) 7WSL-4Z18, (B) 7WSL-2J4Z, (C) 7WSL-4IXP, (D) 7WSL-6IGX, (E) 7WSL-5J0A and (F) 7WSL-2OVJ. The color represents correlation motion, where blue indicates a high correlation and red indicates a negative correlation

cancer cells, inhibiting cancer growth, and preventing cancer.

Dostarlimab and the immune target proteins in the DCCM (dynamic cross-correlation map) were significantly associated with 7WSL-4Z18, 7WSL-2J4Z, 7WSL-4IXP, 7WSL-6IGX, 7WSL-5J0A, and 7WSL-2OVJ (Fig. 6A-F). The cross-correlation matrix, derived from the essential dynamics of MD simulation trajectories, depicted correlated motion, with blue indicating high correlation and red indicating negative correlation. The substantial number of pairwise correlated residues between the immune target proteins and Dostarlimab suggested persistent binding. Subsequent exploration of the conformational states of these systems through PCA and DCCM revealed that the 6 immune

targets and Dostarlimab exhibited a smaller phase space, with significantly reduced negatively correlated movement.

In summary, while our study relies on bioinformatics, its efficacy warrants validation through subsequent *in vitro* tests. Through this research, potential FDA-approved Dostarlimab candidates were identified that potentially have inhibitory effects on immune targets. Additionally, we elucidated conformational differences in immune proteins after binding with Dostarlimab, providing valuable insights for potential cancer prevention strategies, particularly for liver cancer patients.

Discussion

Currently, small molecule-based immunotherapy and target-based personalized medicine focus on cancer patient treatment. Its advantages include higher oral bio-availability, lower cost, and good potential with less toxicity and adverse effects[33]. However, the pharmacokinetics of small molecules have received limited attention due to their ability to mimic regular intracellular protein–protein interactions[34]. The greatest advantage of immune checkpoint inhibitors is that they have attracted much attention, especially for PD1/PDL1 receptor interactions[35]. This computational method could provide unique methods for modeling immune checkpoint inhibitors and immune targets (PD1/PDL1) to predict immune therapeutic treatments[36]. For this analysis, we used big data inputs such as clinical data and genomic data such as transcriptome data. Immunoinformatics analysis was used to predict the immune targets AURKA, MELK, NCAPG, PBK, and RACGAP1. It is essential to determine how immune targets and immune checkpoint inhibitors bind with high affinity and block immune responses by modulating T-cell activity[37].

Dostarlimab (7WSL), derived from a mouse monoclonal antibody (mAb), was humanized by grafting its heavy- and light-chain complementarity-determining regions. Dostarlimab's preclinical assessment showed it to be a promising anti-PD-1 antibody that effectively blocks PD-1 interaction with PD-L1 and PD-L2, akin to established therapies[33]. In addition to Dostarlimab, otherPD-1/PDL1 inhibitors, such as Pembrolizumab, Nivolumab, and Atezolizumab, have shown significant efficacy in various oncological settings. While Dostarlimab has demonstrated promising results, especially in certain patient populations, it is essential to compare its therapeutic potential with these established agents. For example, Pembrolizumab has a broader range of FDA-approved indications, and Nivolumab has been widely studied in combination therapies, potentially offering advantages in specific cases. The available clinical data on response rates, survival outcomes, and safety profiles to provide a comprehensive overview. This comparative analysis highlights that while Dostarlimab is a valuable addition to the therapeutic arsenal, the choice of PD-1/PDL1 inhibitor should be guided by patient-specific factors, tumor characteristics, and prior treatment history. By situating Dostarlimab within the broader landscape of PD-1/PDL1 inhibitors, we aim to present a more balanced and nuanced evaluation of its potential [38].

Our investigation focused on assessing the therapeutic potential of ICI compounds such as Dostarlimab (7WSL) for the selective inhibition of the target genes PDL1 (4Z18), AURKA (2J4Z), MELK (4IXP), NCAPG (6IGX), PBK (5J0A), and RACGAP1 (2OVJ). Through molecular docking and dynamics simulation studies, we explored the therapeutic viability of the screened compounds. These target genes, which are strongly upregulated in various cancers and are associated with poor overall survival, were the targets of interest. Molecular docking and dynamic analyses demonstrated the potency of Dostarlimab as a target gene inhibitor, as Dostarlimab exhibited increased binding affinity and stability, findings consistent with the results of molecular dynamics simulations[39,40].

The docking interactions between 7WSL and 2J4Z and between 7WSL and 4IXP resulted in a high binding affinity of -466.9 kcal/mol. AURKA up-regulation in multiple cancers correlated with poorer overall and relapse-free survival. Molecular docking and dynamic analysis identified two new drug analogs as potent AURKA inhibitors with superior binding affinities and stabilities. The expression profiles and prognostic significance of AURKA across various cancers have been explored, and structurally similar compounds have been explored for selective AURKA inhibition[41]. The missing hydrogen atoms, loop segments, and residues were reconstructed. MELK levels (-466.9 kcal/mol) were found to be correlated with low overall survival and disease-free survival in lung cancer patients. Moreover, molecular modeling indicated its potential binding site for the catalytic domain of MELK[42].

The binding affinities of 7WSL and 6IGX were -460.2 kcal/mol[43]. The binding affinities of 7WSL, 5JOA and 7WSL-2OVJ were 435.1 kcal/mol. Henceforth, directing efforts toward PBK RACGAP1 could emerge as a pivotal strategy in both cancer prevention and therapy. Consequently, the present review aims to scrutinize and assess the significance of PBK and RACGAP1 as potential drug targets in cancer treatment while delineating recent discoveries regarding their involvement in tumor progression. Additionally, this review offers a comprehensive outlook on the advancements made in discovering and formulating PBK inhibitors, with an eye toward prospective clinical utilization[44,45]. Overall, the binding affinities of 7WSL and 4Z18 were 433.9 kcal/mol (Table 2), while compared with all other targets, the effectiveness of the PDL1 core immune target was reduced, and the combination of these five immune targets could potentially be effective for treating HCC patients[46].

The MD simulation of the system timeframe was 100 ns, and the structural changes during the simulation of the RMSD and RMSF values were calculated. 7WSL-4Z18 exhibited the highest average RMSD of 5.064 Å, indicating a greater degree of structural fluctuation during the MD simulation. The RMSD values of the antigen (2J4Z, 4IXP, 6IGX, 5J0A, 2OVJ) and antibody (7WSL) complexes exhibited various degrees of binding stability. The RMSD and standard deviation of the complex with antigens exhibited stability with MD simulations. The most stable antigens were 7WSL-2J4Z, 7WSL-4IXP and 7WSL-2OVJ, whose RMSD values ranged from 4.463 Å to 4.972 Å and 3.942 Å, respectively, with standard deviations ranging from 0.657 Å to 1.001 Å and 0.697 Å, respectively. The less stable binding complexes were 7WSL-6IGX and 7WSL-5J0A, with RMSD values of 10.317 Å and 8.512 Å, respectively, which are greater than the standard deviations of 1.566 Å and 1.036 Å, respectively (Fig. 2).

The RMSF values, which represent the local structural dynamics of the antibody (PDB ID: 7WSL) when bound to different antigens during a 100 ns MD simulation, indicate the flexibility and stability of the antibody-antigen complexes. The complex antigens 7WSL-4Z18, 7WSL-2J4Z 7WSL-4IXP, 7WSL-2OVJ, 7WSL-6IGX and 7WSL-5J0A (Figs 3 and 4) could have different impacts on the dynamics of antigen and antibody interactions during molecular dynamics simulations, and this complex system may respond to immune reactions in various cancers. PCA and DCCM serve as robust analytical tools applied in MD simulations to gain insights into the dynamics and correlated movements within biomolecular systems, such as those involved in antigen–antibody interactions, facilitating a deeper comprehension of their behavior and functional properties. PCA reduces data dimensionality while preserving variance, which is crucial in MD simulations for analyzing biomolecular conformational dynamics and identifying dominant motions and correlated fluctuations. Computing the covariance matrix from trajectory data reveals how each motion mode influences the overall system dynamics. PC1 and PC2 typically capture (Fig. 5) significant fluctuations, aiding in discerning collective motions, conformational changes, or correlated fluctuations within biomolecular systems, such as domain movements or inter-regional interactions[47]. DCCM analyses correlated motions among residue or atom pairs in MD simulations, offering insight into biomolecular system dynamics over time. Correlation coefficients are organized into a dynamic cross-correlation matrix, where each element signifies motion correlation between specific residues or atoms. In Figure 6, which is visualized as a heatmap, blue denotes positive (high) correlations, indicating synchronized motions, while red indicates negative correlations, representing opposite movements[48].

Conclusion

This study emphasizes the importance of computational methods for predicting and understanding immune interactions, providing valuable insights for future experimental and clinical studies. The findings also highlight the potential of Dostarlimab as an immune checkpoint inhibitor for liver cancer, and novel immune targets present promising avenues for further exploration and therapeutic development. The comprehensive analysis of docking and molecular dynamics simulations revealed interactions between the antibody Dostarlimab (PDB ID: 7WSL) and various antigens, including known targets such as PDL1 (4Z18) and novel targets (AURKA, MELK, NCAPG, PBK, and RACGAP1). The docking analysis highlighted specific clusters with the lowest energy for each antigen-antibody complex, indicating favorable binding interactions. The detailed examination of intermolecular interactions in protein–protein docking studies revealed key residues involved in hydrogen bonding, salt bridges, and

clashes. These interactions play a crucial role in stabilizing the complexes and influencing the binding affinity. Notably, Tyr 100 and Asp 33 on the heavy chain, as well as Thr 94 on the light chain, were frequently involved in interactions across different antigen–antibody complexes.

From the molecular dynamics simulations, the RMSD values provided insights into the stability of the complexes over a 100 ns timeframe. Antigen-antibody complexes with AURKA, MELK, NCAPG, PBK, and RACGAP1 exhibited varying degrees of stability, with 7WSL-2OVJ showing the lowest average RMSD, indicating a relatively stable interaction. In contrast, 7WSL-4Z18 demonstrated the highest average RMSD, suggesting more dynamic binding. The RMSF values further delved into the local structural dynamics, highlighting differences in flexibility among the complexes. Antigen-antibody complexes with 7WSL-4IXP displayed reduced local fluctuations, while 7WSL-6IGX exhibited greater flexibility. Comparing these results with the RMSF values of the antibody alone revealed how each antigen influenced the local dynamics. In the context of immune checkpoint inhibitors, Dostarlimab demonstrated good binding affinity and stability across all antigen-antibody complexes, suggesting its potential as an effective immune checkpoint inhibitor for activating T cells and inducing immune responses. The analysis of novel immune targets (AURKA, MELK, NCAPG, PBK, and RACGAP1) revealed their potential as targets for further investigation in liver cancer treatment.

Acknowledgement

The authors thank DST-SERB and ICMR for providing financial assistance to Dr. Vaddi Damodara Reddy under the Ramanujan Fellowship (SB/S2/RJN-043/2014) and Mrs. Swetha Pulakuntla under the ICMR-Senior Research Fellowship (ISRM/11 (32)/2022) scheme. Authors also thank King Saud University, Riyadh, Saudi Arabia for the financial assistance under Researchers Supporting Project Number RSP2024R371.

Conflict of interest

All authors declare no conflict of interest.

References

1 Ganeshpurkar A, Chaturvedi A, Shrivastava A, Dubey N, Jain S, Saxena N, Gupta P & Mujariya R, *In silico* interaction of Berberine with some immunomodulatory targets: A docking analysis. *Indian J Biochem Biophys*, 59 (2022) 8.

2 Gupta K & Dangi K, Immunomodulatory potential of nanomaterials: Interaction with the immune system. *Indian J Biochem Biophys*, 59 (2022) 1162.

3 Eno J, Immunotherapy through the years. *J Adv Pract Oncol,* 8 (2017) 753.

4 Costa B & Vale N, Dostarlimab: A Review. *Biomolecules*, 12 (2022) 1031.

5 Yu X, Gao R, Li Y & Zeng C, Regulation of PD-1 in T cells for cancer immunotherapy. *Eur J Pharmacol,* 881 (2020) 173240.

6 Wang Y, Zhang H, Liu C, Wang Z, Wu W, Zhang N, Zhang L, Hu J, Luo P, Zhang J, Liu Z, Peng Y, Liu Z, Tang L & Cheng Q, Immune checkpoint modulators in cancer immunotherapy: recent advances and emerging concepts. *J Hematol Oncol*, 15 (2022) 111.

7 Darnell EP, Mooradian MJ, Baruch EN, Yilmaz M & Reynolds KL, Immune-Related Adverse Events (irAEs): Diagnosis, Management, and Clinical Pearls. *Curr Oncol Rep*, 22 (2020) 39.

8 Yi M, Jiao D, Xu H, Liu Q, Zhao W, Han X & Wu K, Biomarkers for predicting efficacy of PD-1/PD-L1 inhibitors. *Mol Cancer*, 17 (2018) 129.

9 Rowshanravan B, Halliday N & Sansom DM, CTLA-4: a moving target in immunotherapy. *Blood*, 131 (2018) 67.

10 Triebel F, Jitsukawa S, Baixeras E, Roman-Roman S, Genevee C, Viegas-Pequignot E & Hercend T, LAG-3, a novel lymphocyte activation gene closely related to CD4. *J Exp Med*, 171 (1990) 1405.

11 Hald SM, Rakaee M, Martinez I, Richardsen E, Al-Saad S, Erna-Elise P, Blix ES, Kilvaer T, Andersen S, Lill-Tove B, Bremnes RM & Donnem T, LAG-3 in Non-Small-cell Lung Cancer: Expression in Primary Tumors and Metastatic Lymph Nodes Is Associated With Improved Survival. *Clin Lung Cancer*, 19 (2018) 259.

12 Wurz GT, Kao CJ & DeGregorio MW, Novel cancer antigens for personalized immunotherapies: latest evidence and clinical potential. *Ther Adv Med Oncol*, 8 (2016) 31.

13 Cercek A, Lumish M, Sinopoli J, Weiss J, Shia J, Lamendola-Essel M, El Dika IH, Segal N, Shcherba M, Sugarman R, Stadler Z, Yaeger R, Smith JJ, Rousseau B, Argiles G, Patel M, Desai A, Saltz LB, Widmar M, Iyer K, Zhang J, Gianino N, Crane C, Romesser PB, Pappou EP, Paty P, Garcia-Aguilar J, Gonen M, Gollub M, Weiser MR, Schalper KA & Diaz Jr LA, PD-1 Blockade in Mismatch Repair-Deficient, Locally Advanced Rectal Cancer. *N Engl J Med*, 386 (2022) 2376.

14 Cicala CM, Musacchio L, Scambia G, Lorusso D, Dostarlimab: From preclinical investigation to drug approval and future directions. *Hum Vaccin Immunother*, 19 (2023) 2178220.

15 Babar Q, Saeed A, Murugappan S, Dhumal D, Tabish T, Thorat ND, Promise of dostarlimab in cancer therapy: Advancements and cross-talk considerations. *Drug Discov Today*, 28 (2023) 103577.

16 Markham A, Dostarlimab: First Approval. *Drugs*, 81 (2021) 1213.

17 Park UB, Jeong TJ, Gu N, Lee HT, Heo YS, Molecular basis of PD-1 blockade by dostarlimab, the FDA-approved antibody for cancer immunotherapy. *Biochem Biophys Res Commun*, 599 (2022) 37.

18 Patnaik A, Weiss GJ, Rasco DW, Blaydorn L, Mirabella A, Beeram M, Guo W, Lu S, Danaee H, McEachern K, Im E &

Sachdev JC, Safety, antitumor activity, and pharmacokinetics of dostarlimab, an anti-PD-1, in patients with advanced solid tumors: a dose-escalation phase 1 trial. *Cancer Chemother Pharmacol*, 89 (2022) 103.

19 Tacrolimus, In: *LiverTox: Clinical and Research Information on Drug-Induced Liver Injury*. Bethesda (MD): National Institute of Diabetes and Digestive and Kidney Diseases; 17, 2020.

20 Mirza MR, Chase DM, Slomovitz BMdePont R, Novák Z, Black D, Gilbert L, Sharma S, Valabrega G, M Landrum L, Hanker LC, Stuckey A, Boere I, Gold MA, Auranen A, Pothuri B, Cibula D, McCourt C, Raspagliesi F, Shahin MS, Gill SE, Monk BJ, Buscema J, Herzog TJ, Copeland LJ, Tian M, He Z, Stevens S, Zografos E, Coleman RL, Powell MA & RUBY Investigators, Dostarlimab for Primary Advanced or Recurrent Endometrial Cancer. *N Engl J Med*, 388 (2023) 2145.

21 Varadharajan V, Ganapathi ST, Mandal SK, Prediction of protein-protein interaction networks and druggable genes associated with Parkinson's disease. *Indian J Biochem Biophys*, 59 (2022) 49.

22 Pulakuntla S, Singh SA & Reddy VD, Hub gene identification and immune infiltration analysis in hepatocellular carcinoma: Computational approach. *In silico pharmacolog,* 12 (2024) 39.

23 Coudert E, Gehant S, de Castro E, Pozzato M, Baratin D, Neto T, Sigrist CJA, Redaschi N, Bridge A & UniProt Consortium, Annotation of biologically relevant ligands in UniProtKB using ChEBI. *Bioinformatics*, 39 (2023) 793.

24 Doytchinova IA, Flower DR, VaxiJen: a server for prediction of protective antigens, tumour antigens and subunit vaccines. *BMC Bioinformatics*, 8 (2007) 4.

25 Waterhouse A, Bertoni M, Bienert S, Studer G, Tauriello G, Gumienny R, Heer FT, de Beer TAP, Rempfer C, Bordoli L, Lepore R & Schwede T, SWISS-MODEL: homology modelling of protein structures and complexes. *Nucleic Acids Res*, 46 (2018) W296.

26 Reynisson B, Alvarez B, Paul S, Peters B, Nielsen M, NetMHCpan-4.1 and NetMHCIIpan-4.0: improved predictions of MHC antigen presentation by concurrent motif deconvolution and integration of MS MHC eluted ligand data. *Nucleic Acids Res*, 48 (2020) 454.

27 Desta IT, Porter KA, Xia B, Kozakov D, Vajda S, Performance and Its Limits in Rigid Body Protein-Protein Docking. *Structure*, 28 (2020) 1081.

28 Phillips JC, Hardy DJ, Maia JDC, Stone JE, Ribeiro JV, Bernardi RC, Buch R, Fiorin G, Hénin J, Jiang W, McGreevy R, Melo MCR, Radak BK, Skeel RD, Singharoy A, Wang Y, Roux B, Aksimentiev A, Luthey-Schulten Z, Kalé LV, Schulten K, Chipot C & Tajkhorshid E, Scalable molecular dynamics on CPU and GPU architectures with NAMD. *J Chem Phys*, 153 (2020) 044130.

29 Pulakuntla S, Lokhande KB, Padmavathi P, Pal M, Swamy KV, Sadasivam J, Singh SA, Aramgam SL & Reddy VD, Mutational analysis in international isolates and drug repurposing against SARS-CoV-2 spike protein: molecular docking and simulation approach. *Virus Dis*, 32 (2021) 702.

30 Grant BJ, Skjaerven L, Yao XQ, The Bio3D packages for structural bioinformatics. *Protein Sci*, 30 (2021) 30.

31 Ganjipour G, Heshmati M, Hashemi M & Entezari M, Administration of Curcumin, Betanin, and CoQ10 combined with nickel oxide, iron superoxide nanoparticles show preventive effects in breast cancer: Effect on apoptosis pathway and MiR-455 expression. *Indian J Biochem Biophys*, 60 (2023) 790.

32 Bulik-Sullivan B, Busby J, Palmer CD, Davis MJ, Murphy T, Clark A, Busby M, Duke F, Yang A, Young L, Ojo NC, Caldwell K, Abhyankar J, Boucher T, Hart MG, Makarov V, De Montpreville VT, Mercier O, Chan TA, Scagliotti G, Bironzo P, Novello S, Karachaliou N, Rosell R, Anderson I, Gabrail N, Hrom J, Limvarapuss C, Choquette K, Spira A, Rousseau R, Voong C, Rizvi NA, Fadel E, Frattini M, Jooss K, Skoberne M, Francis J & Yelensky R, Deep learning using tumor HLA peptide mass spectrometry datasets improves neoantigen identification. *Nat Biotechnol*, 1038 (2018) 4313

33 DiFrancesco M, Hofer J, Aradhya A, Rufinus J, Stoddart J, Finocchiaro S, Mani J, Tevis S, Visconti M, Walawender G, DiFlumeri J, Fattakhova E & Patil SP, Discovery of small-molecule PD-1/PD-L1 antagonists through combined virtual screening and experimental validation. *Comp Biol Chem,* 102 (2023) 107804.

34 Wells JA & McClendon CL, Reaching for high-hanging fruit in drug discovery at protein–protein interfaces. *Nature,* 450 (2007) 1009.

35 Jain S, Prajapati H, Ganeshpurkar A, Dubey N, Singh S, Computational Insights into the interaction of Piperine with Immune Regulatory Proteins: A Docking Study *Indian J Biochem Biophys*, 60 (2023) 484.

36 Lombardo SD, Presti M, Mangano K, Petralia MC, Basile M. S, Libra M, Candido S, Fagone P, Mazzon E, Nicoletti F & Bramanti A, Prediction of PD-L1 Expression in Neuroblastoma *via* Computational Modeling. *Brain Sci,* 9 (2019) 221.

37 Melhem, M., Hanze, E., Lu, S., Alskär, O., Visser, S., & Gandhi, Y, Population pharmacokinetics and exposure-response of anti-programmed cell death protein-1 monoclonal antibody dostarlimab in advanced solid tumors. *Br J Clin Pharmacol,* 88 (2022) 4154.

38 Kumar S, Ghosh S, Sharma G, Wang Z, Kehry MR, Marino MH, Neben TY, Lu S, Luo S, Roberts S, Ramaswamy S, Danaee H & Jenkins D, Preclinical characterization of dostarlimab, a therapeutic anti-PD-1 antibody with potent activity to enhance immune function in *in vitro* cellular assays and *in vivo* animal models. *Mabs,* 13 (2021) 1954136.

39 Kumar A, Mishra T, Kulshreshtha A, Binding interaction of laccases from Bacillus subtilis after industrial dyes exposure: Molecular docking and molecular dynamics simulation studies. *Indian J Biochem Biophys*, 60 (2023) 320.

40 Gonzalez-Sapienza G, Rossotti MA & Tabares-da Rosa S, Single-Domain Antibodies As Versatile Affinity Reagents for Analytical and Diagnostic Applications. *Front Immunol,* 8 (2017) 977.

41 Almilaibary A, Targeting aurora kinase a (AURKA) in cancer: molecular docking and dynamic simulations of potential AURKA inhibitors. *Med Oncol,* 39 (2022) 246.

42 Li H, Chen M, Yang Z, Wang Q, Wang J, Jin D, Yang X, Chen F, Zhou X & Luo K, Phillygenin, a MELK Inhibitor,

Inhibits Cell Survival and Epithelial–Mesenchymal Transition in Pancreatic Cancer Cells. *Onco Targets Ther,* 13 (2020) 2842.

43 Xiao C, Gong J, Jie Y, Cao J, Chen Z, Li R, Chong Y, Hu B & Zhang Q, NCAPG Is a Promising Therapeutic Target Across Different Tumor Types. *Front Pharmacol,* 11 (2020) 387.

44 Huang H, Lee MH, Liu K, Dong Z, Ryoo Z & Kim MO, PBK/TOPK: An Effective Drug Target with Diverse Therapeutic Potential. *Cancers,* 13 (2021) 2232.

45 Wu X, Xu Z, Li W, Lu Y & Pu J, HIF-1α and RACGAP1 promote the progression of hepatocellular carcinoma in a mutually regulatory way. *Mol Med Rep,* 28 (2023) 218.

46 Kamal MA, Badary HA, Omran D, Shousha HI, Abdelaziz AO, El Tayebi HM & Mandour YM, Virtual Screening and Biological Evaluation of Potential PD-1/PD-L1 Immune Checkpoint Inhibitors as Anti-Hepatocellular Carcinoma Agents. *ACS Omega,* 8 (2023) 33254.

47 David CC, Jacobs DJ, Principal component analysis: a method for determining the essential dynamics of proteins. *Methods Mol Biol*, 1084 (2014) 226.

48 Arnold GE, Ornstein RL, Molecular dynamics study of time-correlated protein domain motions and molecular flexibility: cytochrome P450BM-3. *Biophys J*, 73 (1997) 1159.